THE JOURNAL OF PHYSICAL CHEMISTRY C
A JOURNAL OF THE AMERICAN CHEMICAL SOCIETY

pubs.acs.org/JPCC
Article

Toward an ab Initio Description of Adsorbate Surface Dynamics

Published as part of The Journal of Physical Chemistry C virtual special issue "Jens K. Nørskov Festschrift".

Saurabh Sivakumar and Ambarish Kulkarni*

Cite This: *J. Phys. Chem. C* 2024, 128, 13238−13248
Read Online

ABSTRACT: The advent of machine learning potentials (MLPs) provides a unique opportunity to access simulation time scales and to directly compute physicochemical properties that are typically intractable using density functional theory (DFT). In this study, we use an active learning curriculum to train a generalizable MLP using the DeepMD-kit architecture. By using sufficiently long MLP-based molecular dynamics (MD) simulations, which provide DFT-level accuracy, we investigate the diffusion of key surface-bound adsorbates on a Ag(111) facet. Detailed analysis of the MLP/MD-calculated diffusivities sheds light on the potential shortcomings of using DFT-based nudged elastic band to estimate surface diffusion barriers. More generally, while this study is focused on a specific system, we anticipate that the underlying workflows and the resulting models can be extended to other adsorbates and other materials in the future.

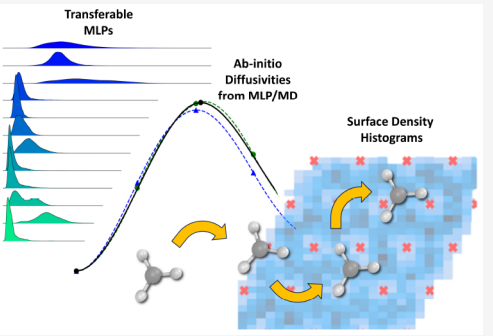

INTRODUCTION

Pioneered by Prof. Jens Nørskov and co-workers in their early works, descriptor-based analyses have now become an indispensable tool used by researchers within the heterogeneous catalysis community.[1−5] This philosophy is based on the hypothesis that appropriately identified descriptors, which are often binding energies of key intermediates, can help in rationalizing experimentally observed trends across catalyst compositions, thereby accelerating the design of novel functional materials for the target reaction. The continuing impact of Prof. Nørskov's contributions in this field is evidenced by several recent reviews on these topics.[6−10]

A defining characteristic of this Nørskovian-philosophy is the ability to describe the complexity of multistep reactions, often involving several surface-bound intermediates, using just one or two adsorption-based descriptors. Historically, this simplification was necessary to alleviate the computational costs of calculating hundreds of reaction barriers for every elementary step, and then repeating this process for several different catalyst compositions.[11−15] Indeed, the concept of linear scaling relationships, which is based on the well-known bond order conservation principle, now forms the core vocabulary used within this field.[16,17]

Although the calculation of reaction barriers remains cumbersome, recent work by us and others has demonstrated how machine learning potentials (MLPs) can be used to overcome this bottleneck.[18−22] For instance, using Cu-exchanged zeolites as a prototypical example, we have explicitly calculated the transition state geometries and reaction barriers of methane activation for thousands of $[CuOCu]^{2+}$sites across 52 zeolites. While most sites show linear trends between the C−H activation barrier and the H binding energy, our analysis identifies several important factors (e.g., confinement and accessibility) that cause deviation from the expected universal scaling behavior.[23] Similarly, building upon the foundation provided by scaling relationships, other groups have proposed novel strategies to further improve the accuracy of these approximations.[24−27]

Analogous to how the development of MLPs has simplified the calculation of reaction barriers, in this study, we focus on the related but less explored phenomena of surface diffusion. Indeed, surface phenomena such as adsorption, diffusion, and desorption of molecular and atomic adsorbates are of wide interest in the field of catalysis.[28,29] Several studies have shown that slow diffusion processes can have a significant impact on the overall rate of catalytic reactions.[30,31] While the typical approach within the field relies on using nudged elastic band calculations and harmonic transition state theory (hTST) to estimate diffusion barriers,[20,32,33] here, we propose an alternative strategy that uses sufficiently long MLP-based molecular dynamics simulations to measure adsorbate diffusivities without making any prior assumptions about the preferred diffusion pathway. Specifically, we calculate temperature-dependent diffusivities of 8 commonly studied adsorbates using Ag(111) as an example of an industrially relevant catalyst.[34,35] We choose to focus on Ag

Received: April 5, 2024
Revised: July 8, 2024
Accepted: July 18, 2024
Published: July 27, 2024

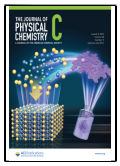

https://doi.org/10.1021/acs.jpcc.4c02250
J. Phys. Chem. C 2024, 128, 13238−13248

because of its efficacy in catalyzing selective oxidation reactions. We are particularly inspired by detailed molecular beam mass spectroscopy studies reported by Zhou et al.[36,37] for methanol oxidation. We use a learning curriculum that combines ab initio molecular dynamics (AIMD) simulations of gas-phase species along with AIMD simulation of the bound adsorbates to obtain a transferable DeepMD-Kit-based model.[38−40] Importantly, we also show that the resulting model is easily transferable to related species that were not included in the original training data set. Similar approaches have shown demonstrable success for studying diverse materials including zeolites and MOFs, and for investigating N_2 adsorption on Fe surfaces.[41−43] Taken together, this study highlights the wide versatility and growing relevance of MLP-based approaches in investigating phenomena that are typically not possible using traditional DFT simulations.

METHODS

DFT Calculations. Our MLP development protocol involves several different types of DFT calculations. We use single-point energy evaluations (DFT/SPE), geometry optimizations (DFT/OPT) and ab initio molecular dynamics (AIMD) simulations. All DFT calculations are performed using the Vienna ab initio simulation package (VASP).[44,45] We use the RPBE functional[46] with Grimme's D3 dispersion corrections using a Becke-Johnson damping scheme.[47−49] We note that this workflow uses DFT data obtained using the RBPE functional as a reference as it has been shown to provide good accuracy-to-cost trade-offs.[50,51] However, we acknowledge that several recent studies have demonstrated the potential shortcomings of the Grimme's D3 method.[52,53] Although not explored here, we emphasize that this workflow is generalizable and can also be used with newer VdW-DF2 based functionals. A plane wave energy cutoff of 500 eV is used. Ionic relaxation steps are terminated when the forces on all atoms are less than 0.05 eV/Å. Our AIMD simulations are performed within an NVT ensemble using the Nose-Hoover thermostat.[54]

MLP Development. A 2-stage iterative approach is used for MLP development. Stage A uses a series of short AIMD simulations (298 K, 2,000 steps, 0.5 fs time step) of 678 gas-phase adsorbates obtained as their SMILES notation from Reuter et al.[55] (27,000 configurations, Γ-point only) along with AIMD simulations of these adsorbates bound to a constrained 1-layer Ag(111) slab (27,000 configurations). All slab calculations use 4 × 4 × 1 k-points with >10 Å vacuum spacing between periodic images in the z-direction. These AIMD configurations are sampled every 50 steps to obtain an initial DFT training data set. RDKit[56] and the Atomic Simulation Environment (ASE)[57] are used to streamline the workflows. We emphasize that the 1-layer slab model is physically unrealistic. However, the DFT data from these simulations provides a useful preliminary MLP model (denoted as DP_0^{prelim}) to accelerate subsequent active learning iterations in Stage B.

Model Parameters and Training. DeepPot-SE[38,40] as implemented within the DeepMD-kit framework is used as the MLP architecture. Similar to our previous studies,[23,58] we use 3-layer embedding (i.e., 16/32/64) and fitting nets (i.e., 64/64/64). The distance cutoff radius of 6.0 Å with smoothing beginning at 5.5 Å is used. Our DP models are trained for 8×10^7 steps. The initial learning rate is set to 0.001, which exponentially decays to 3.5×10^{-10}. The prefactors for the energy and force contributions to the loss function are p_e^{start} = 0.02, p_e^{limit} = 1, p_f^{start} = 1000, and p_f^{limit} = 1. A standard test-train split of 80% (training), 10% (validation) and 10% (test) is used. We note that the model hyperparameters chosen here have not been optimized. Further performance improvements, possible with hyperparameter tuning, are beyond the scope of this study.

Additionally, we acknowledge that any of the several publicly available MLP models, which have been pretrained on larger DFT data sets, could have been used here instead of DeepMD-kit.[59−62] While these architectures may show better performance in predicting energies and/or forces, previous work by Jaakkola et al.[63] emphasizes the importance of using predicted physicochemical properties (e.g., diffusivity) as a metric of model performance. Thus, we focus on the DeepMD-kit architecture due to its simple LAMMPS interface and relatively fast CPU-based model training iterations.

Active Learning Protocol. We use an active learning approach for model refinement. For example, MD configurations obtained from the i^{th} DP model (i.e., DP_i/MD, 400 K, 2 ns, 0.5 fs time step, using LAMMPS) are down-selected based on their estimated model uncertainties. Similar to previous work by us[23,58] and others,[64,65] we use the ϵ_t metric to quantify model uncertainty. Here, ϵ_t for a given configuration $\boldsymbol{R}_t$ is defined by eq 1

$$\epsilon_t = \max_j \sqrt{\langle \left\| F_{w,j}(\boldsymbol{R}_t) - \langle F_{w,j}(\boldsymbol{R}_t) \rangle \right\|^2 \rangle} \tag{1}$$

where $F_{w,j}$ denotes the force on the atom with index j predicted by the model w. This metric measures the maximum standard deviation in force predictions obtained using an ensemble of models.[65] Here, we use an ensemble of 4 models differing in the seed value used to initialize the weights of the neural nets. This uncertainty quantification approach underpins our active learning protocol.

Diffusivity Calculations. Molecular dynamics simulations are used to calculate the self-diffusivities of several Ag-bound adsorbates. LAMMPS[66] is used as the MD simulation engine as it interfaces smoothly with DeepMD-kit. Specifically, we perform 2 ns NVT MD simulations (0.2 ns equilibration, 0.5 fs time step) at three different temperatures (300 K, 350 and 400 K). The resulting unwrapped coordinates are used to calculate a windowed mean square displacement (MSD) as a function of all possible lag-times using eq 2. Here, $\vec{r}_i$ refers to the positions of the atoms at time t, m is the lag-time ($m < m_{max}$, the length of the MD trajectory), and N is the maximum number of possible lag times. This averaging strategy mitigates the MSD fluctuations that arise due to the small number of diffusing species in our system.[67,68] All MSD-based analyses use the open-source MDAnalysis toolkit.[69,70]

$$MSD(m) = \frac{1}{N_{particles}} \sum_{i=1}^{N_{particles}} \frac{1}{N-m} \sum_{k=0}^{N-m-1} (\vec{r}_i(k+m) - \vec{r}_i(k))^2 \tag{2}$$

The self-diffusion coefficient for each adsorbate is obtained using the slope of a linear fit to MSD vs lag time plot using eq 3. As we focus on surface diffusion (i.e., in x and y directions), the dimensionality parameter (d in eq 3) is set to 2 in our analysis.

$$D = \frac{1}{2d} \lim_{t\to\infty} \frac{\mathrm{d}}{\mathrm{d}t}(MSD(m)) \tag{3}$$

The self-diffusion coefficients obtained from MSD analyses are used to calculate activation energies using the Arrhenius eq 4

https://doi.org/10.1021/acs.jpcc.4c02250
J. Phys. Chem. C 2024, 128, 13238−13248

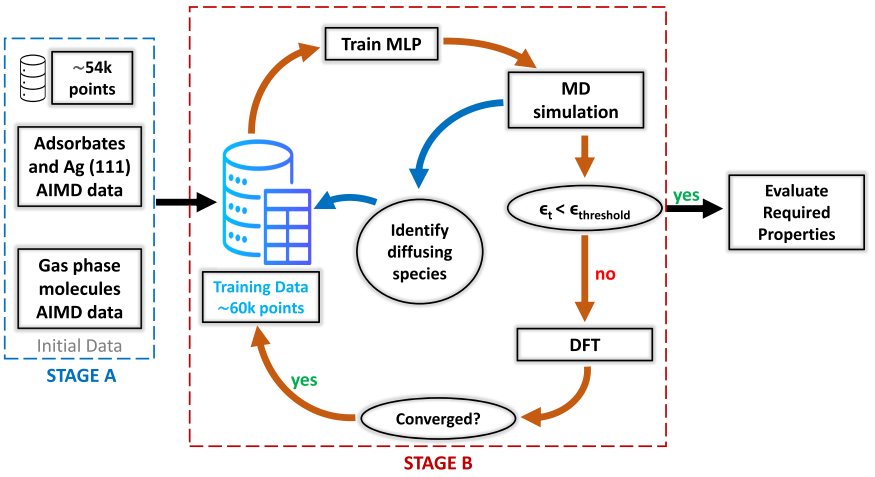

Figure 1. Overview of the 2-stage model development and evaluation protocol. Stage A is trained on ∼54,000 configurations of gas phase and the adsorbates on 1 layer; Stage B adds another ∼6,000 configurations to the stage A data set. The orange arrows show active learning loops. The blue arrows show steps exclusively involving the DP_0^{prelim} model.

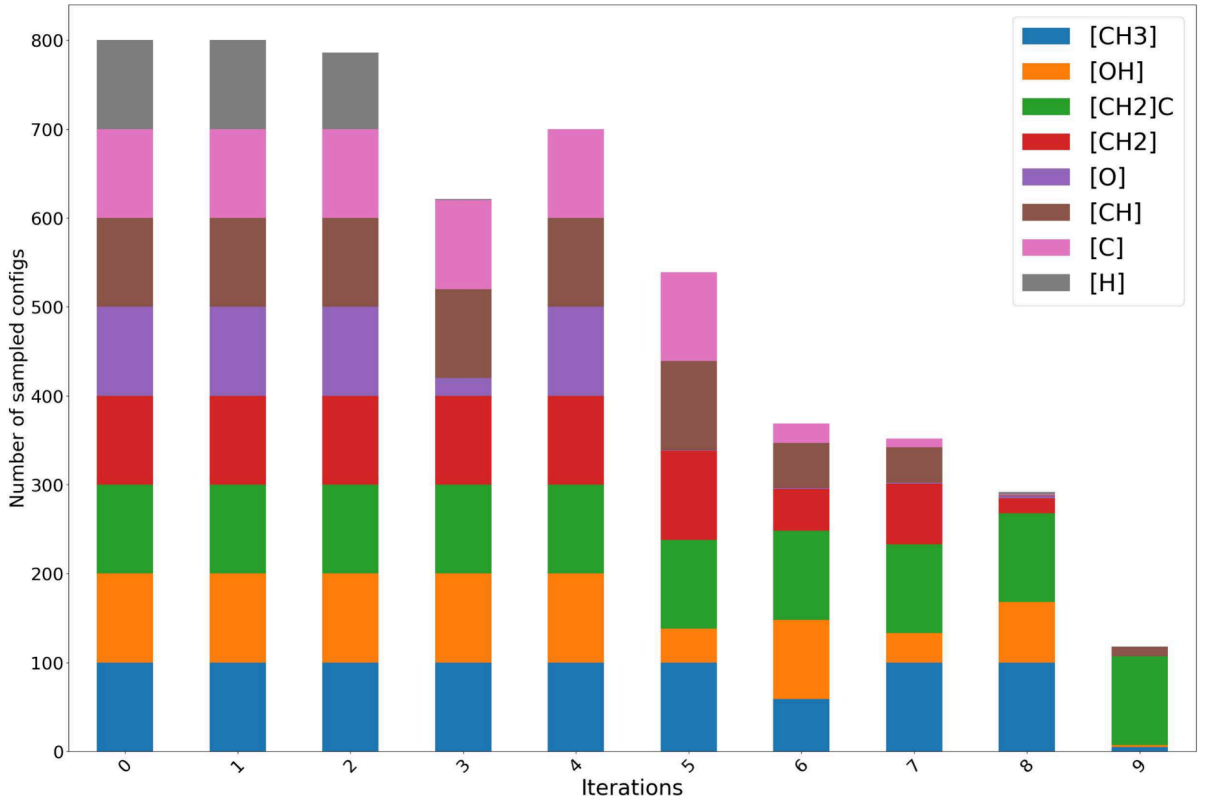

Figure 2. Number of adsorbate configurations added at each step of the active learning protocol. The adsorbates are denoted using their SMILES representation.

$$D = D_0 \exp\left(\frac{-E_d^{app}}{k_B T}\right) \tag{4}$$

where E_d^{app} is the apparent diffusion energy barrier, k_B is the Boltzmann constant and D_0 is the pre-exponential factor. As shown in 5, D_0 includes the attempt frequency and entropic effects associated with the diffusion process.[71]

$$D_0 = \frac{n_p \nu_0 l^2}{2d} \tag{5}$$

Here, n_p is the number of equivalent diffusion paths, l is the jump length, and ν_0 is the attempt/jump frequency of the adsorbate that is related to their vibrational free energies.[72,73]

RESULTS AND DISCUSSION

Model Development. The DP_0^{prelim} MLP obtained from Stage A, which is trained using gas-phase and 1-layer Ag slab data, serves as a starting point for subsequent model iterations. First, we performed MLP-based molecular dynamics (i.e., DP_0^{prelim}/MD) simulations (NVT ensemble, 400 K, 0.2 ns, 0.5 fs time step) for all 678 adsorbates using the 1-layer Ag slab.

https://doi.org/10.1021/acs.jpcc.4c02250
J. Phys. Chem. C 2024, 128, 13238−13248

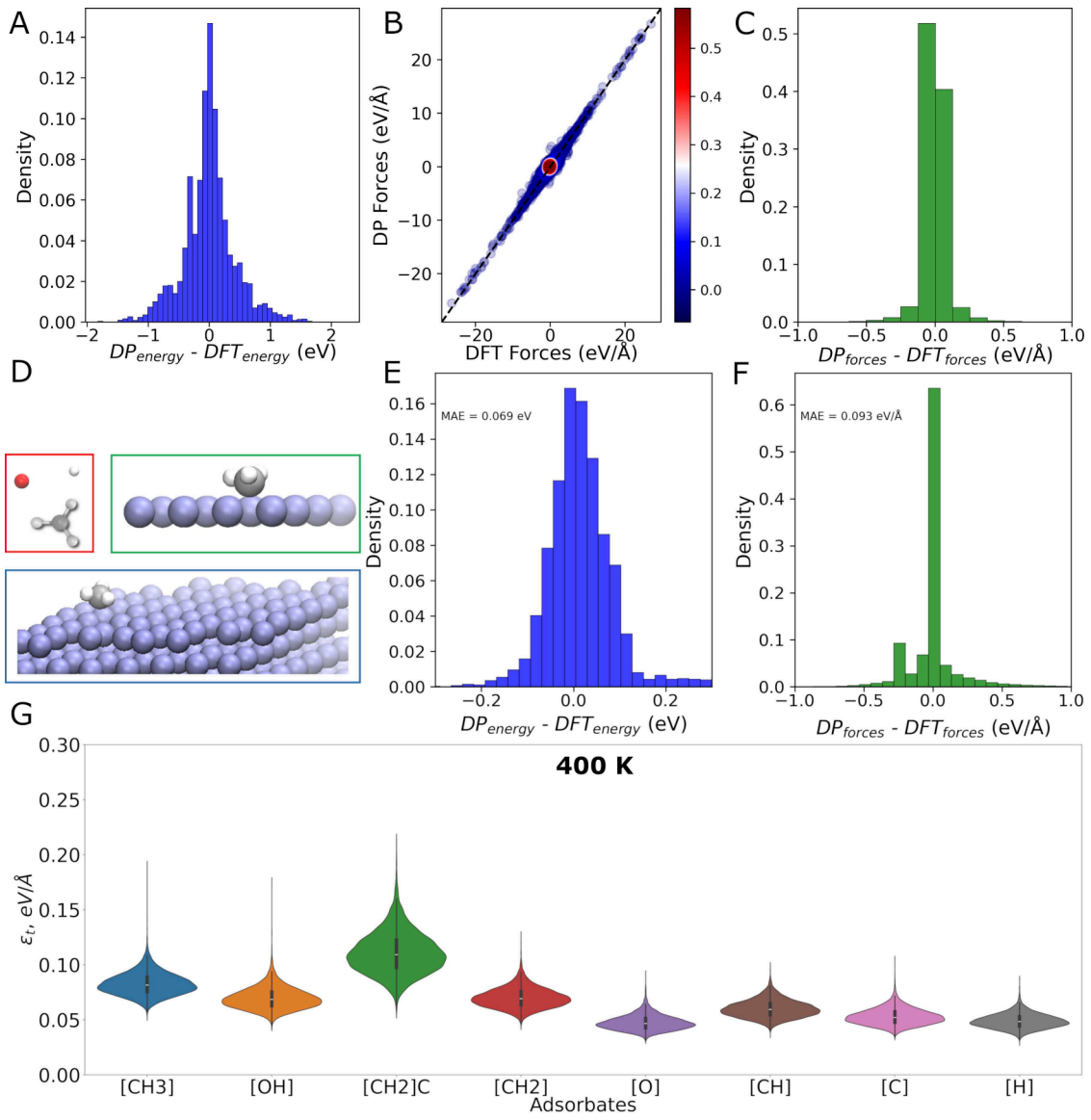

Figure 3. (A) Histogram of the energy differences (Model predicted energies − DFT energies) on the test data set. (B) Parity plot of the forces on the test data set. (C) Histogram of the force differences on the test data set (Model predicted forces − DFT forces) within −1 to 1 eV/Å. (D) Schematic of types of structures used in training the models. Red box: Selected gas phase adsorbates. Green box: Adsorbate on a single layer of Ag. Blue box: Adsorbate on 4 layers of Ag. (E) Histogram of the energy residuals on the test data set consisting of only adsorbates on a 4 layer slab. (F) Histogram of the force residuals on the data set consisting of only adsorbates on a 4 layer slab. (G) Averaged ϵ_t over 5 repeats of a 2 ns MD simulation at 400 K for all adsorbates (denoted by their SMILES representation). The upper limit on the *y*-axis (0.3 ev/Å) is the termination criteria.

These preliminary simulations are used to identify adsorbates that desorb or disintegrate within our short simulation time scales. Examples of this behavior are shown in the SI (Figure S1). Since the overall goal of this work is to investigate surface diffusion, we shortlisted 20 adsorbates with 3 or fewer C atoms that stably diffuse over 0.2 ns (Table S1). Of these, we chose a subset of 8 adsorbates (i.e., CH_3, OH, CH_3CH_2, CH_2, CH, O, C, H), which are relevant for a wide class of reactions, for the diffusion studies discussed below. We acknowledge using a 1-layer slab model, which is helpful in quickly shortlisting a set of adsorbate molecules for model refinement, open the possibility that other adsorbates that are unstable on a single layer Ag slab could be stable (i.e., remain intact) when using a traditional 4-layer model. Although such adsorbates are not explored in more detail, we anticipate that our final diffusion model can be extended easily to other adsorbates of interest. This is demonstrated for CHOH ads in the later sections of this work.

These 8 adsorbates are placed on an on-top site of a 4-layer Ag(111) slab; the bottom 2 layers are constrained. These structures are optimized using DFT, and similar to what is described above, short AIMD simulations (298 K, 2,000 steps, 0.5 fs time step) are used to obtain 100 new configurations for each adsorbate. These data are combined with the Stage A data set to obtain the next iteration of the model. As shown in Figure 1, this process is repeated until the ϵ_t metric is smaller than a threshold value. The final model obtained after 10 iterations (i.e., DP_{10}) of stage B shows an $\epsilon_t < 0.3$ eV/Å.

The computational efficiency of the above MLP development protocol depends on the sampling strategy used to select configurations for DFT/SPE calculations. In this work, we employ a wider sampling range compared to previous

https://doi.org/10.1021/acs.jpcc.4c02250
J. Phys. Chem. C 2024, 128, 13238−13248

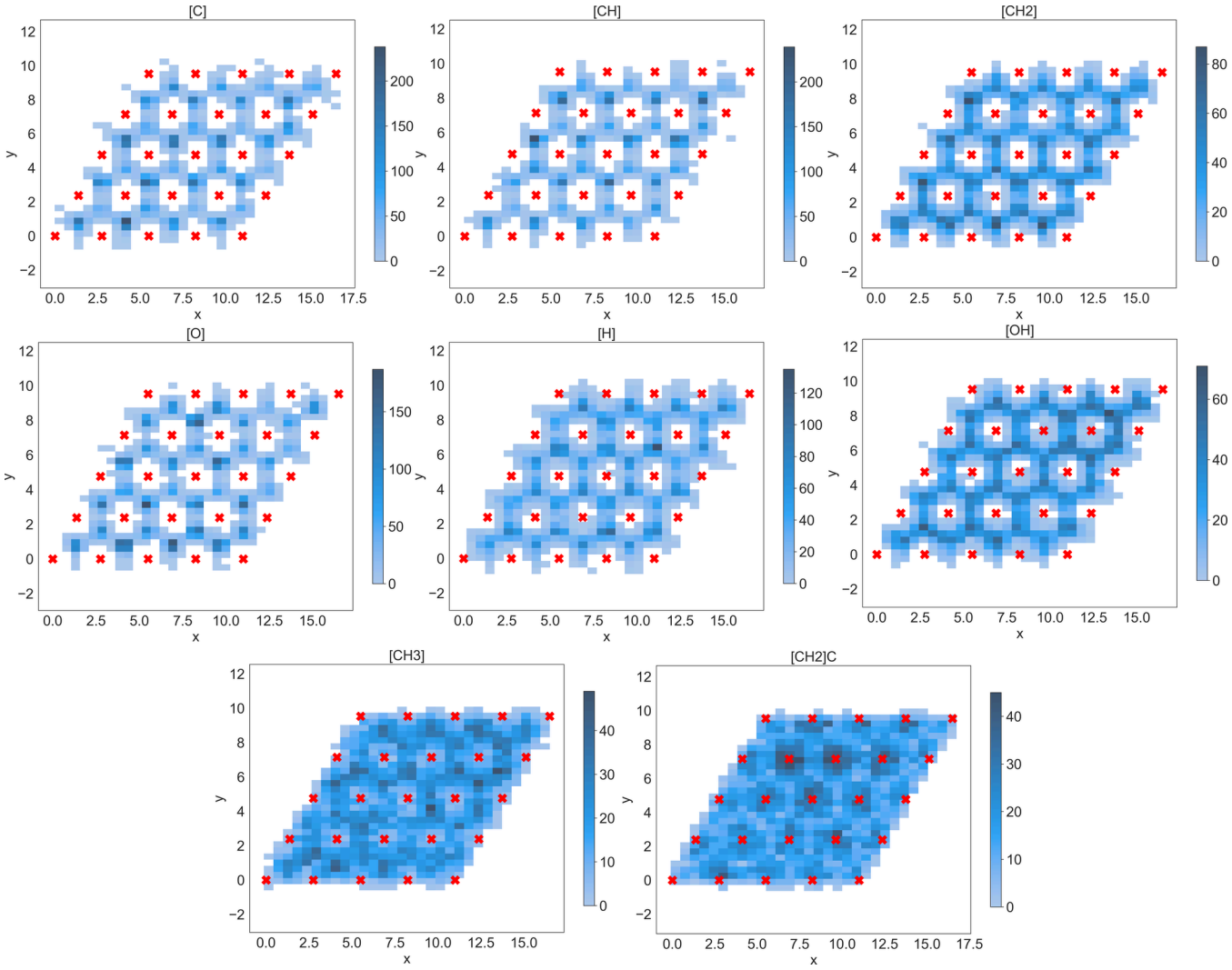

Figure 4. Adsorbate surface density histograms of the diffusing adsorbates (denoted by SMILES in the titles). The red ×'s denote the positions of the Ag atoms for the 111 facet.

studies.[23,58,64] Specifically, we use 0.2 eV/Å and 0.7 eV/Å as the lower and upper ϵ_t bounds for sampling, respectively. Within these bounds, configurations from the MD trajectory are randomly sampled to obtain a maximum of 100 possible configurations for each adsorbate. If fewer than 100 configurations lie within the chosen ϵ_t bounds, then all available configurations are used for DFT/SPE. To minimize sampling of configurations that are already well described by the model, a tighter sampling procedure (0.3−0.7 eV/Å) was used for the final two iterations.

The number of configurations sampled for each adsorbate during the training curriculum is shown in Figure 2. The first few iterations of our active learning protocol result in uniform sampling across different adsorbates. However, as expected, we observe that the number of configurations sampled per iteration decreases during model training. Ethyl requires the largest number of iterations and sampled configurations to converge. Taken together, the final DP_{10} model is trained on ∼27,000 gas-phase, ∼ 27,000 1-layer and ∼6,000 4-layer DFT data points. Although not used here, we note that analogous workflows can now be implemented through the DPGen interface.[65]

Model Performance. Figures 3A-C show the performance of the final DP_{10} model for the test data set. The MLP-predicted energies and forces show good agreement with DFT; we observe mean absolute errors (MAEs) of 0.3 eV (for energies) and 0.04 eV/Å (forces). To further test the predictive power of the model, we ran 2 ns MD simulations for all 8 adsorbates at 3 different temperatures using LAMMPS (NVT ensemble, 0.5 fs time step, 0.2 ns equilibration, 5 repeats). Our results, shown as ϵ_t violin plots in Figure 3G for the 400 K run, show predicted model uncertainties are well below the 0.3 eV/Å threshold. Analogous analysis for the other temperatures is shown in the SI (Figure S2). Furthermore, we selected 300 configurations for each adsorbate from these repeats for evaluation with DFT and used those data to evaluate the energy and force residuals of the model on the adsorbate behavior on the 4-layer Ag system. These results are shown as histograms in Figure 3E-F. The model has an MAE of 0.07 eV (energies) and 0.09 eV/Å (forces) on the adsorbate +4-layer Ag system. Taken together, this analysis confirms the ability of the model to reliably access simulation time scales (>2 ns) that are typically inaccessible with DFT.

Adsorbate Surface Density Histograms. To further emphasize the value of the above MD simulations, Figure 4 compares the adsorbate surface density histograms for all 8 diffusing species obtained from 2 ns MD simulations performed

https://doi.org/10.1021/acs.jpcc.4c02250
J. Phys. Chem. C 2024, 128, 13238−13248

at 400 K. Here, the adsorbate surface density is calculated by analyzing the MLP/MD trajectories and averaging the site occupancy using a 0.57 Å × 0.57 Å grid. We observe that atomic species such as C, H and O remain localized to the 3-fold sites, with lower occupancy of the bridge sites, and an almost complete exclusion of the on-top positions. In contrast, other species (e.g., methyl, hydroxyl and ethyl) diffuse more freely across the entire surface. These trends, which are correlated with the denticity of the adsorbates, suggest that the diffusion of (say) methyl on Ag(111) could follow several different pathways. As shown in Figure S13, we find that the pathways for diffusion of methyl on Ag each have relatively accessible barriers. These observations are consistent with the surface density plots shown in Figure 4. On the other hand, the diffusion of O and other atomic adsorbates is largely limited to an activated hopping step across the bridge sites. As hTST/NEB-based diffusivity calculations have historically focused on studying specific diffusion pathways, the results in Figure 4 could have important implications on the accuracy of hTST/NEB estimates, especially for weakly bound species such as methyl. In particular, as our MLP/MD-based diffusivity calculations are not restricted to any predefined diffusion paths and do not rely on the harmonic approximation, we believe that the following MD-based investigation provides a more realistic description of adsorbate diffusion on metal surfaces.

Diffusivity Trends and Diffusion Barriers. Table 1 shows the diffusion coefficients calculated using eq 3 at three different temperatures for the 8 adsorbates considered here. An example of the MSD fitting procedure is shown in Figure 5A. Consistent with increased adsorbate mobility at higher temperatures, we obtain larger diffusion coefficients at 400 K compared to 300 and 350 K. Comparing across different adsorbates, we observe that methyl shows the highest diffusivity (2.38×10^{-7} m^2/s at 400 K) that is about 2 orders of magnitude higher than strongly bound adsorbates such as C, O and CH.[74] The diffusivity of other species (i.e., H, OH, CH_2, and ethyl) lies in between these two extremes.

Table 1. Diffusivites of Adsorbates at 400, 350, and 300 K, E_d^{app} (Apparent Diffusion Barrier) Calculated from the Arrhenius Relation, and the Intercept as Shown in eq 4

Adsorbate[a]	Diffusivity (400 K) × 10^{-9} (m^2/s)	Diffusivity (350 K) × 10^{-9} (m^2/s)	Diffusivity (300 K) × 10^{-9} (m^2/s)	E_d^{app} (eV)	Intercept ($\ln(D_0)$)
[CH3]	238.63	149.57	46.34	0.18	8.70
[CH2]	30.25	17.63	13.68	0.08	3.35
[CH]	3.42	3.06	1.06	0.12	2.71
[C]	2.07	1.46	0.94	0.08	0.80
[O]	3.97	2.16	0.95	0.14	3.37
[H]	44.17	32.73	16.03	0.11	4.61
[OH]	27.51	16.94	13.85	0.07	2.94
[CH2]C	67.34	57.84	33.71	0.07	4.07

[a]Adsorbates are denoted using their SMILES representation.

Using eq 4, the temperature-dependent diffusion coefficients are used to obtain apparent activation energies for the overall diffusion process. Consistent with the adsorbate surface density histograms discussed previously, we observe near-perfect Arrhenius behavior for the atomic adsorbates (Figure 5B.) As shown in Figure S3, slightly larger deviations are observed for molecular adsorbates. While deviation from Arrhenius behavior is observed across multiple repeats, at this stage, the atomistic origin of these trends remains unclear.

Consistent with previous DFT-based studies,[74] we note that the calculated diffusion barrier for CH_3 (i.e., E_d^{app} = 0.18 eV) is higher than that for CH_2 (0.08), CH (0.12) and C (0.08). However, CH_3 is the most mobile species, where the higher diffusivity is due to a much larger pre-exponential factor for methyl (i.e., $e^{8.7}$)compared to other adsorbates, suggesting a larger contribution arising from the entropic effects. Although not explicitly included in the Arrhenius form, we hypothesize that these trends can be rationalized based on the higher attempt to diffuse frequency of CH_3 as shown in eq 5.[71,72]

Specifically, eqs 4 and 5 show that the rate of surface diffusion is correlated with the diffusion jump length and attempt frequency. Thus, it is interesting to note that C shows low diffusivity despite a small diffusion barrier. We hypothesize that this behavior is likely due to a lower jump frequency for C as evidenced by the lowest intercept across the 8 adsorbates considered here. This suggests that carbon rarely jumps between the stable sites and using an Arrhenius-type framework to analyze the MLP/MD diffusivities results in a surprisingly low value of the apparent diffusion barrier (i.e., E_d^{app}). Similarly, analogous arguments can be used to explain the higher E_d^{app} for CH compared to C. Here, CH shows a higher attempt to diffuse frequency than C, as shown previously by Chen et al.[74] this is likely because of fewer valence electrons that are available to interact with the Ag surface.

More generally, this discussion highlights the advantages of using MD simulations (rather than a hTST framework) for investigating trends in surface diffusion across different adsorbates. Specifically, since E_d^{app} intrinsically includes a

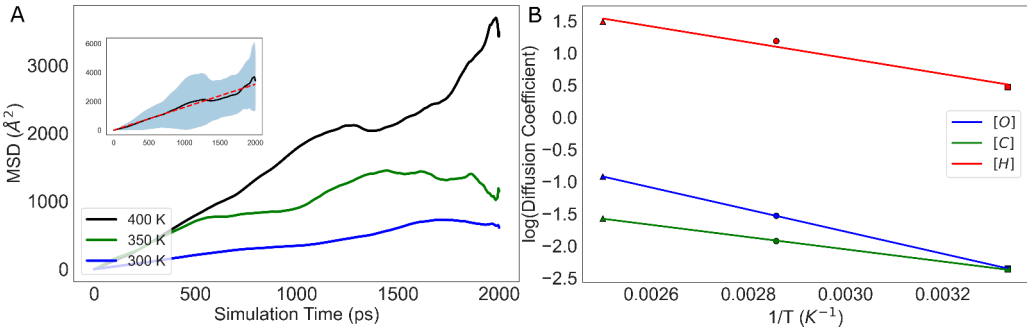

Figure 5. (A) Window MSD computed over 2 ns for Oxygen on Ag (111) for 400, 350, and 300 K. The inset shows the linear fit (dashed red line) for 400 K with the hue indicating the average standard deviation of the squared distances. (B) Arrhenius plots for atomic adsorbates on Ag (111). △ represents 400 K; ○ represents 350 K; □ represents 300 K.

https://doi.org/10.1021/acs.jpcc.4c02250
J. Phys. Chem. C 2024, 128, 13238−13248

measure of the diffusion attempt frequency and is not restricted to a particular pathway as would be the case with an NEB, we believe that the MLP/MD-derived values reported in Table 1 are more accurate than NEB-based estimates.

Furthermore, as a point of comparison with traditional NEB-based studies, we used the DP_{10} model to run an NEB calculation. Specifically, using O as a prototypical example, we compare the apparent diffusion energy barrier obtained from the MD simulation to the one that is obtained from a NEB calculation. We studied the diffusion of O from the most stable fcc site[74] to the hcp site on Ag (111). As shown in Figure 6, we

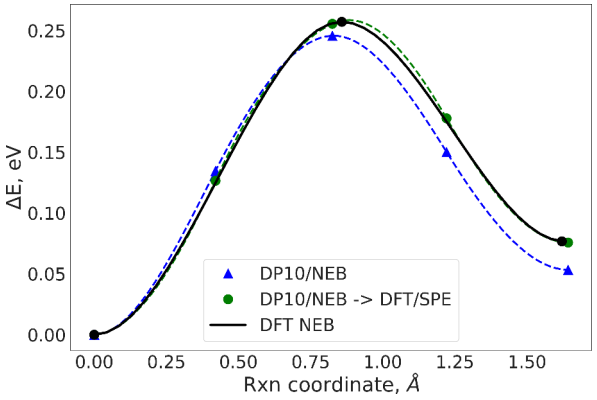

Figure 6. Comparison of DP_{10}/NEBs, DP_{10}/SPE NEBs, and DFT NEBs for O diffusing from fcc to hcp via a bridge site on Ag (111).

observe a small energy mismatch between the DFT-predicted barrier and ML-predicted barrier. This is likely due to the higher total energy MAEs, and model training being more focused on reproducing DFT-forces. Although not discussed here, we note that the energy accuracy can be improved via hyperparameter optimization.

These discrepancies however do not impact the overall conclusions of this study as the xyz coordinates obtained from MLP-based NEB are in excellent agreement with DFT calculations. For instance, single point energy calculations on MLP/NEB-derived geometries are almost identical with full DFT/NEB optimization across the entire reaction coordinate (Figure 6). We observe that the barrier predicted from MD (from Table 1) is ∼0.11 eV lower than the barrier evaluated for the fcc to hcp path explored using NEB. As previously mentioned, this difference likely stems from the fact that our calculated E_d^{app} implicitly accounts for all possible diffusion pathways while an NEB calculation does not. A more detailed analysis of this result using the ensemble of DP_{10} models is provided in the SI (Figure S12).

Model Convergence. All the above diffusion studies are based on data obtained using the final DP_{10} model. However, the active learning curriculum used for model training allows us to compare the trends in model performance and reliability across different training iterations.[23] As shown in Figure 7 and the violin plots in S4−11, we observe a general trend where the rate of model convergence is correlated with the chemical complexity of the adsorbate. For instance, Figure 7 compares the model uncertainty (as measured by ϵ_t) over multiple training iterations for O and OH. While the model learns to describe the dynamics of atomic adsorbates such as O (Figure 7A) in a few iterations, more complex behavior is observed for OH (Figure 7B). Specifically, the MD simulation using the iteration 2 model (i.e.,

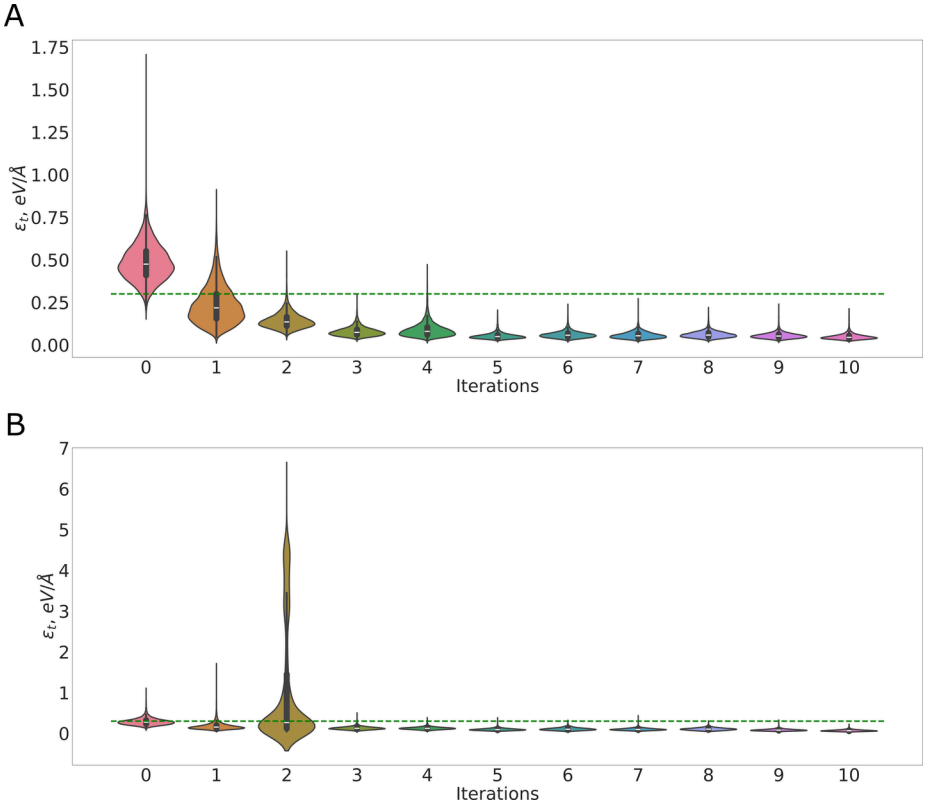

Figure 7. Violin plot of ϵ_t over model training iterations for (A) O and (B) OH. The horizontal green lines represent ϵ_t = 0.3 eV/Å, which is used as the model convergence criteria.

https://doi.org/10.1021/acs.jpcc.4c02250
J. Phys. Chem. C 2024, 128, 13238−13248

DP_2/MD) explores a wider configuration space resulting in a higher ϵ_t than the previous iteration, which is then well described in the subsequent DP_3 model. This ability to self-correct is also observed for ethyl (Figure S5) and is a major advantage of using a curriculum-based training approach.[23] Specifically, we observe that ethyl requires the longest number of iterations to converge, which is also reflected in the higher number of sampled configurations across all training iterations (Figure 2). Similar plots and trends for the other adsorbates can be found in the SI (Figures S4−S11). While it is possible that graph-based MLP architectures may require fewer training data,[63,75] these comparisons are beyond the scope of this work.

Model Transferability. To assess the efficacy and generalizability of our training protocol, we now explore the transferability of the model to an adsorbate that was not included during Stage B training. We focus on [CHOH] as it is an important surface intermediate for methanol partial oxidation and CO_2 reduction reactions.[76−78] Furthermore, [CHOH] is interesting as it includes several different types of bonds (i.e., C−H, O−H, and C−O) and has a local bonding environment that is similar to the 8 adsorbates considered above.

Figure 8 summarizes the model performance for [CHOH] as measured by the ϵ_t metric across the various training iterations.

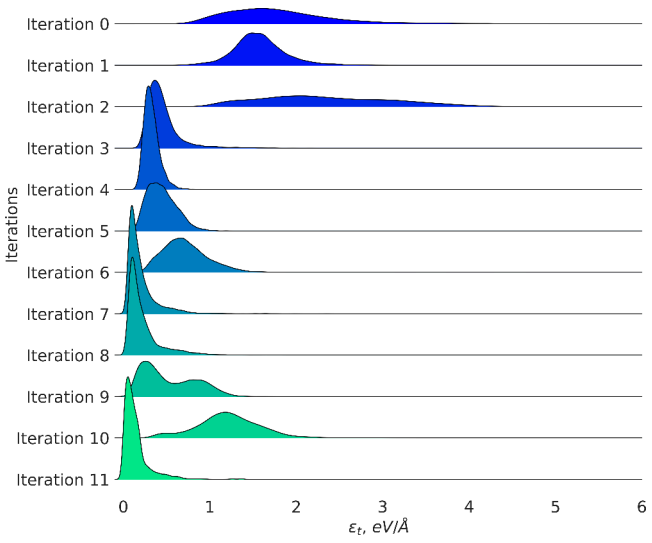

Figure 8. Assessing the model transferable to previously unseen adsorbates using the ϵ_t metric. Iteration 11 of the model was fine-tuned using 100 DFT data points for [CHOH].

In contrast to progressive improvements (i.e., decreasing ϵ_t) observed for the 8 adsorbates (Figures S4−S11 violinplots), the ϵ_t metric for [CHOH] shows an oscillatory behavior. Specifically, we observe consistent improvements until iteration 4, which is followed by slightly diminished performance after iteration 5 and 6. These trends of improving (iteration 6 and 7) and worsening (iteration 9 and 10) model uncertainty are repeated over the subsequent iterations, which suggests the inability of the model to consistently describe the dynamics of [CHOH].

The above trends are not surprising since the model has not been exposed to any DFT data for the [CHOH] adsorbate after stage A. Thus, similar to the process used above, we subsequently perform a single retraining step using DFT/SPEs for 100 [CHOH] configurations obtained using DP_{10}/MD. As shown by iteration 11 in Figure 8, this leads to a drastic improvement in the ϵ_t metric, thereby demonstrating the ability to fine-tune this model to previously unseen adsorbates. Although beyond the scope of this study, we anticipate that the final DP_{10} model, which is available in the SI, can be generalized to other adsorbates using small quantities of DFT-training data.

CONCLUSIONS

In summary, this work demonstrates an active learning approach for developing transferable machine learning-based potential (MLP) that can be used to study surface diffusion phenomena at ab initio accuracy. The active learning approach facilitates on-the-fly identification of configurations for iterative model refinement - a strategy that is particularly advantageous for modeling the dynamics of complex adsorbates bound to metal surfaces. To illustrate this workflow, we have investigated the surface diffusion of 8 commonly studied adsorbates abound to a prototypical Ag(111) facet. While the current version of the MLP does not include adsorbate−adsorbate interactions, we anticipate that this model can be further augmented to include these important phenomena by using appropriate DFT data sets. The resulting diffusivity trends, obtained from molecular dynamics simulations and by fitting mean square displacements, highlight the potential shortcomings of using traditional NEB-based calculations to estimate diffusion barriers. Furthermore, our resulting model demonstrates good transferability and can be easily fine-tuned to study other unseen adsorbates by simply including small amounts of additional DFT data. Thus, in the future, we anticipate these workflows and the resulting models can be easily generalized to other adsorbates, metals, and facets.

ASSOCIATED CONTENT

Supporting Information

The Supporting Information is available free of charge at https://pubs.acs.org/doi/10.1021/acs.jpcc.4c02250.

Additional results and details; Figure S1, the tendency of certain adsorbates to desorb/split rather than diffuse; Figure S2, the variation of ϵ_t at 300 and 350 K; Figure S3, the Arrhenius plot for molecular adsorbates; Figures S4−S11, MSD, Arrhenius behavior, and variation of ϵ_t over AL iterations for all adsorbates; Figure S12, calculated NEB using ensemble of DP models for O diffusing from FCC to HCP on Ag (111); Figure S13, calculated diffusion barriers; Table S1, adsorbates denoted by their SMILES; Table S2, diffusivites of adsorbates (PDF)

AUTHOR INFORMATION

Corresponding Author

Ambarish Kulkarni − *Department of Chemical Engineering, University of California, Davis, California 95616, United States;* orcid.org/0000-0001-9834-8264; Email: arkulkarni@ucdavis.edu

Author

Saurabh Sivakumar − *Department of Chemical Engineering, University of California, Davis, California 95616, United States*

Complete contact information is available at: https://pubs.acs.org/10.1021/acs.jpcc.4c02250

Notes

The authors declare no competing financial interest.

VASP INCAR files for generating AIMD configurations, LAMMPS inputs for calculating diffusivity (in.atoms, data.atoms) using DeepMD MLP, Training data (data), the trained model (graph.pb), and the associated model parameters (in.json) are available on github: https://github.com/kul-group/Ag_diffusion_data

■ ACKNOWLEDGMENTS

This work was supported by the U.S. Department of Energy (DOE), Office of Basic Energy Sciences(BES), Division of Chemical Sciences, Geosciences and Biosciences (CSGB) under Grant DE-SC0020320. This research used resources of the National Energy Research Scientific Computing Center (NERSC), a U.S. Department of Energy Office of Science User Facility located at Lawrence Berkeley National Laboratory, operated under Contract No. DE-AC02-05CH11231. S.S. thanks Trevor Price and Sudheesh Ethirajan for valuable discussions on this topic.

■ REFERENCES

(1) Nørskov, J.; Bligaard, T.; Logadottir, A.; Bahn, S.; Hansen, L.; Bollinger, M.; Bengaard, H.; Hammer, B.; Sljivancanin, Z.; Mavrikakis, M.; et al. Universality in Heterogeneous Catalysis. *J. Catal.* **2002**, *209*, 275−278.
(2) Nørskov, J. K.; Bligaard, T.; Logadottir, A.; Kitchin, J. R.; Chen, J. G.; Pandelov, S.; Stimming, U. Trends in the Exchange Current for Hydrogen Evolution. *J. Electrochem. Soc.* **2005**, *152*, J23.
(3) Logadottir, A.; Rod, T.; Nørskov, J.; Hammer, B.; Dahl, S.; Jacobsen, C. The Brønsted−Evans−Polanyi Relation and the Volcano Plot for Ammonia Synthesis over Transition Metal Catalysts. *J. Catal.* **2001**, *197*, 229−231.
(4) Greeley, J.; Jaramillo, T. F.; Bonde, J.; Chorkendorff, I.; Nørskov, J. K. Computational high-throughput screening of electrocatalytic materials for hydrogen evolution. *Nat. Mater.* **2006**, *5*, 909−913.
(5) Nørskov, J. K.; Abild-Pedersen, F.; Studt, F.; Bligaard, T. Density functional theory in surface chemistry and catalysis. *Proc. Natl. Acad. Sci. U. S. A.* **2011**, *108*, 937−943.
(6) Liu, J.; Wang, Z.; Kou, L.; Gu, Y. Mechanism Exploration and Catalyst Design for Hydrogen Evolution Reaction Accelerated by Density Functional Theory Simulations. *ACS Sustainable Chem. Eng.* **2023**, *11*, 467−481.
(7) Chen, B. W. J.; Xu, L.; Mavrikakis, M. Computational Methods in Heterogeneous Catalysis. *Chem. Rev.* **2021**, *121*, 1007−1048.
(8) Goldsmith, B. R.; Esterhuizen, J.; Liu, J.-X.; Bartel, C. J.; Sutton, C. Machine learning for heterogeneous catalyst design and discovery. *AIChE J.* **2018**, *64*, 2311−2323.
(9) Motagamwala, A. H.; Ball, M. R.; Dumesic, J. A. Microkinetic Analysis and Scaling Relations for Catalyst Design. *Annu. Rev. Chem. Biomol. Eng.* **2018**, *9*, 413−450.
(10) Zhao, Z.-J.; Liu, S.; Zha, S.; Cheng, D.; Studt, F.; Henkelman, G.; Gong, J. Theory-guided design of catalytic materials using scaling relationships and reactivity descriptors. *Nature Reviews Materials* **2019**, *4*, 792−804.
(11) Latimer, A. A.; Aljama, H.; Kakekhani, A.; Yoo, J. S.; Kulkarni, A.; Tsai, C.; Garcia-Melchor, M.; Abild-Pedersen Ab, F.; Nørskov, J. K. Mechanistic insights into heterogeneous methane activation †. *Phys. Chem. Chem. Phys.* **2017**, *19*, 3575−3581.
(12) Greeley, J.; Nørskov, J. K.; Mavrikakis, M. ELECTRONIC STRUCTURE AND CATALYSIS ON METAL SURFACES. *Annu. Rev. Phys. Chem.* **2002**, *53*, 319−348.
(13) Nørskov, J. K.; Bligaard, T.; Rossmeisl, J.; Christensen, C. H. Towards the computational design of solid catalysts. *Nat. Chem.* **2009**, *1*, 37−46.
(14) Hammer, B.; Nørskov, J. *Impact of Surface Science on Catalysis*; Advances in Catalysis; Academic Press, 2000; Vol. *45*; pp 71−129.
(15) Jones, G.; Jakobsen, J. G.; Shim, S. S.; Kleis, J.; Andersson, M. P.; Rossmeisl, J.; Abild-Pedersen, F.; Bligaard, T.; Helveg, S.; Hinnemann, B.; et al. First principles calculations and experimental insight into methane steam reforming over transition metal catalysts. *J. Catal.* **2008**, *259*, 147−160.
(16) Medford, A. J.; Vojvodic, A.; Hummelshøj, J. S.; Voss, J.; Abild-Pedersen, F.; Studt, F.; Bligaard, T.; Nilsson, A.; Nørskov, J. K. From the Sabatier principle to a predictive theory of transition-metal heterogeneous catalysis. *J. Catal.* **2015**, *328*, 36−42 (Special Issue: The Impact of Haldor Topsøe on Catalysis).
(17) Greeley, J. Theoretical Heterogeneous Catalysis: Scaling Relationships and Computational Catalyst Design. *Annu. Rev. Chem. Biomol. Eng.* **2016**, *7*, 605−635.
(18) Singh, A. R.; Rohr, B. A.; Gauthier, J. A.; Nørskov, J. K. Predicting Chemical Reaction Barriers with a Machine Learning Model. *Catal. Lett.* **2019**, *149*, 2347−2354.
(19) Schreiner, M.; Bhowmik, A.; Vegge, T.; Busk, J.; Winther, O. Transition1x - a dataset for building generalizable reactive machine learning potentials. *Scientific Data* **2022**, *9*, 1−9.
(20) Peterson, A. A. Acceleration of saddle-point searches with machine learning. *J. Chem. Phys.* **2016**, *145*, 1.
(21) Stocker, S.; Jung, H.; Csányi, G.; Goldsmith, C. F.; Reuter, K.; Margraf, J. T. Estimating Free Energy Barriers for Heterogeneous Catalytic Reactions with Machine Learning Potentials and Umbrella Integration. *J. Chem. Theory Comput.* **2023**, *19*, 6796−6804.
(22) Margraf, J. T.; Jung, H.; Scheurer, C.; Reuter, K. Exploring catalytic reaction networks with machine learning. *Nature Catalysis* **2023**, *6*, 112−121.
(23) Guo, J.; Sours, T.; Holton, S.; Sun, C.; Kulkarni, A. R. Screening Cu-Zeolites for Methane Activation Using Curriculum-Based Training. *ACS Catal.* **2024**, *14*, 1232−1242.
(24) Ulissi, Z. W.; Medford, A. J.; Bligaard, T.; Nørskov, J. K. To address surface reaction network complexity using scaling relations machine learning and DFT calculations. *Nat. Commun.* **2017**, *8*, 14621.
(25) Jenkins, A. H.; Musgrave, C. B.; Medlin, J. W. Altering Linear Scaling Relationships on Metal Catalysts via Ligand-Adsorbate Hydrogen Bonding. *J. Phys. Chem. C* **2021**, *125*, 23791−23802.
(26) Pérez-Ramírez, J.; López, N. Strategies to break linear scaling relationships. *Nature Catalysis* **2019**, *2*, 971−976.
(27) Pablo-García, S.; García-Muelas, R.; Sabadell-Rendón, A.; López, N. Dimensionality reduction of complex reaction networks in heterogeneous catalysis: From linear-scaling relationships to statistical learning techniques. *WIREs Computational Molecular Science* **2021**, *11*, e1540.
(28) Schlexer Lamoureux, P.; Winther, K. T.; Garrido Torres, J. A.; Streibel, V.; Zhao, M.; Bajdich, M.; Abild-Pedersen, F.; Bligaard, T. Machine Learning for Computational Heterogeneous Catalysis. *ChemCatChem.* **2019**, *11*, 3581−3601.
(29) Ma, S.; Liu, Z.-P. Machine Learning for Atomic Simulation and Activity Prediction in Heterogeneous Catalysis: Current Status and Future. *ACS Catal.* **2020**, *10*, 13213−13226.
(30) Antczak, G.; Ehrlich, G. Jump processes in surface diffusion. *Surf. Sci. Rep.* **2007**, *62*, 39−61.
(31) Motagamwala, A. H.; Dumesic, J. A. Microkinetic Modeling: A Tool for Rational Catalyst Design. *Chem. Rev.* **2021**, *121*, 1049−1076.
(32) Henkelman, G.; Uberuaga, B. P.; Jónsson, H. Climbing image nudged elastic band method for finding saddle points and minimum energy paths. *J. Chem. Phys.* **2000**, *113*, 9901−9904.
(33) Henkelman, G.; Jónsson, H. Improved tangent estimate in the nudged elastic band method for finding minimum energy paths and saddle points. *J. Chem. Phys.* **2000**, *113*, 9978−9985.
(34) Li, W.-X.; Stampfl, C.; Scheffler, M. Why is a Noble Metal Catalytically Active? The Role of the O-Ag Interaction in the Function of Silver as an Oxidation Catalyst. *Phys. Rev. Lett.* **2003**, *90*, 256102.
(35) Stegelmann, C.; Schiødt, N.; Campbell, C.; Stoltze, P. Microkinetic modeling of ethylene oxidation over silver. *J. Catal.* **2004**, *221*, 630−649.
(36) Gurses, S. M.; Felvey, N.; Filardi, L. R.; Zhang, A. J.; Wood, J.; Benthem, K. v.; Frank, J. H.; Osborn, D. L.; Hansen, N.; Kronawitter, C. X. Constraining reaction pathways for methanol oxidation through

operando interrogation of both the surface and the near-surface gas phase. *Chem. Catalysis* **2023**, *3*, 100782.
(37) Zhou, B.; Huang, E.; Almeida, R.; Gurses, S.; Ungar, A.; Zetterberg, J.; Kulkarni, A.; Kronawitter, C. X.; Osborn, D. L.; Hansen, N.; et al. Near-Surface Imaging of the Multicomponent Gas Phase above a Silver Catalyst during Partial Oxidation of Methanol. *ACS Catal.* **2021**, *11*, 155−168.
(38) Zhang, L.; Han, J.; Wang, H.; Car, R.; E, W. Deep Potential Molecular Dynamics: A Scalable Model with the Accuracy of Quantum Mechanics. *Phys. Rev. Lett.* **2018**, *120*, 143001.
(39) Zhang, L.; Wang, H.; Car, R.; E, W. Phase Diagram of a Deep Potential Water Model. *Phys. Rev. Lett.* **2021**, *126*, 236001.
(40) Zhang, L.; Han, J.; Wang, H.; Saidi, W.; Car, R.; E, W. End-to-end Symmetry Preserving Inter-atomic Potential Energy Model for Finite and Extended Systems. *NeurIPS Proceedings*; Advances in Neural Information Processing Systems; 2018.
(41) Liu, S.; Dupuis, R.; Fan, D.; Benzaria, S.; Bonneau, M.; Bhatt, P.; Eddaoudi, M.; Maurin, G. Machine learning potential for modelling H2 adsorption/diffusion in MOFs with open metal sites. *Chem. Sci.* **2024**, *15*, 5294−5302.
(42) Millan, R.; Bello-Jurado, E.; Moliner, M.; Boronat, M.; Gomez-Bombarelli, R. Effect of Framework Composition and NH3 on the Diffusion of Cu+ in Cu-CHA Catalysts Predicted by Machine-Learning Accelerated Molecular Dynamics. *ACS Central Science* **2023**, *9*, 2044−2056.
(43) Bonati, L.; Polino, D.; Pizzolitto, C.; Biasi, P.; Eckert, R.; Reitmeier, S.; Schlögl, R.; Parrinello, M. The role of dynamics in heterogeneous catalysis: Surface diffusivity and N2 decomposition on Fe(111). *Proc. Natl. Acad. Sci. U. S. A.* **2023**, *120*, e2313023120.
(44) Kresse, G.; Furthmüller, J. Efficiency of ab-initio total energy calculations for metals and semiconductors using a plane-wave basis set. *Comput. Mater. Sci.* **1996**, *6*, 15−50.
(45) Kresse, G.; Hafner, J. Ab initio molecular dynamics for liquid metals. *Phys. Rev. B* **1993**, *47*, 558−561.
(46) Hammer, B.; Hansen, L. B.; Nørskov, J. K. Improved adsorption energetics within density-functional theory using revised Perdew-Burke-Ernzerhof functionals. *Phys. Rev. B* **1999**, *59*, 7413−7421.
(47) Smith, D. G. A.; Burns, L. A.; Patkowski, K.; Sherrill, C. D. Revised Damping Parameters for the D3 Dispersion Correction to Density Functional Theory. *J. Phys. Chem. Lett.* **2016**, *7*, 2197−2203.
(48) Grimme, S.; Antony, J.; Ehrlich, S.; Krieg, H. A consistent and accurate ab initio parametrization of density functional dispersion correction (DFT-D) for the 94 elements H-Pu. *J. Chem. Phys.* **2010**, *132*, 154104.
(49) Grimme, S.; Ehrlich, S.; Goerigk, L. Effect of the damping function in dispersion corrected density functional theory. *J. Comput. Chem.* **2011**, *32*, 1456−1465.
(50) Göltl, F.; Murray, E. A.; Tacey, S. A.; Rangarajan, S.; Mavrikakis, M. Comparing the performance of density functionals in describing the adsorption of atoms and small molecules on Ni(111). *Surf. Sci.* **2020**, *700*, 121675.
(51) Szaro, N. A.; Bello, M.; Fricke, C. H.; Bamidele, O. H.; Heyden, A. Benchmarking the Accuracy of Density Functional Theory against the Random Phase Approximation for the Ethane Dehydrogenation Network on Pt(111). *J. Phys. Chem. Lett.* **2023**, *14*, 10769−10778.
(52) Lee, J.-H.; Park, J.-H.; Soon, A. Assessing the influence of van der Waals corrected exchange-correlation functionals on the anisotropic mechanical properties of coinage metals. *Phys. Rev. B* **2016**, *94*, 024108.
(53) Ilawe, N. V.; Zimmerman, J. A.; Wong, B. M. Breaking Badly: DFT-D2 Gives Sizeable Errors for Tensile Strengths in Palladium-Hydride Solids. *J. Chem. Theory Comput.* **2015**, *11*, 5426−5435.
(54) Nose, S. Constant Temperature Molecular Dynamics Methods. *Prog. Theor. Phys. Suppl.* **1991**, *103*, 1−46.
(55) Margraf, J. T.; Reuter, K. Systematic Enumeration of Elementary Reaction Steps in Surface Catalysis. *ACS Omega* **2019**, *4*, 3370−3379.
(56) *RDKit: Open-source cheminformatics*; https://www.rdkit.org; Accessed: 2024−04−05.
(57) Hjorth Larsen, A.; Jørgen Mortensen, J.; Blomqvist, J.; Castelli, I. E; Christensen, R.; Dułak, M.; Friis, J.; Groves, M. N; Hammer, B.ør.; Hargus, C.; Hermes, E. D; Jennings, P. C; Bjerre Jensen, P.; Kermode, J.; Kitchin, J. R; Leonhard Kolsbjerg, E.; Kubal, J.; Kaasbjerg, K.; Lysgaard, S.; Bergmann Maronsson, J.; Maxson, T.; Olsen, T.; Pastewka, L.; Peterson, A.; Rostgaard, C.; Schiøtz, J.; Schutt, O.; Strange, M.; Thygesen, K. S; Vegge, T.; Vilhelmsen, L.; Walter, M.; Zeng, Z.; Jacobsen, K. W; et al. The atomic simulation environment—a Python library for working with atoms. *J. Phys.: Condens. Matter* **2017**, *29*, 273002.
(58) Sours, T. G.; Kulkarni, A. R. Predicting Structural Properties of Pure Silica Zeolites Using Deep Neural Network Potentials. *J. Phys. Chem. C* **2023**, *127*, 1455−1463.
(59) Duval, A.; Schmidt, V.; Miret, S.; Bengio, Y.; Hernández-García, A.; Rolnick, D. *PhAST: Physics-Aware, Scalable, and Task-specific GNNs for Accelerated Catalyst Design*; 2024; https://arxiv.org/abs/2211.12020.
(60) Batatia, I.; Benner, P.; Chiang, Y.; Elena, A. M.; Kovács, D. P.; Riebesell, J.; Advincula, X. R.; Asta, M.; Avaylon, M.; Baldwin, W. J.; et al. *A foundation model for atomistic materials chemistry*; 2024; https://arxiv.org/abs/2401.00096.
(61) Tran, R.; Lan, J.; Shuaibi, M.; Wood, B. M.; Goyal, S.; Das, A.; Heras-Domingo, J.; Kolluru, A.; Rizvi, A.; Shoghi, N.; et al. The Open Catalyst 2022 (OC22) Dataset and Challenges for Oxide Electrocatalysts. *ACS Catal.* **2023**, *13*, 3066−3084.
(62) Zitnick, C. L.; Chanussot, L.; Das, A.; Goyal, S.; Heras-Domingo, J.; Ho, C.; Hu, W.; Lavril, T.; Palizhati, A.; Riviere, M.; et al. *An Introduction to Electrocatalyst Design using Machine Learning for Renewable Energy Storage*; 2020; https://arxiv.org/abs/2010.09435.
(63) Fu, X.; Wu, Z.; Wang, W.; Xie, T.; Keten, S.; Gomez-Bombarelli, R.; Jaakkola, T. *Forces are not Enough: Benchmark and Critical Evaluation for Machine Learning Force Fields with Molecular Simulations*; 2023; https://arxiv.org/abs/2210.07237.
(64) Yang, M.; Bonati, L.; Polino, D.; Parrinello, M. Using metadynamics to build neural network potentials for reactive events: the case of urea decomposition in water. *Catal. Today* **2022**, *387*, 143−149.
(65) Zhang, Y.; Wang, H.; Chen, W.; Zeng, J.; Zhang, L.; Wang, H.; E, W. DP-GEN: A concurrent learning platform for the generation of reliable deep learning based potential energy models. *Comput. Phys. Commun.* **2020**, *253*, 107206.
(66) Thompson, A. P.; Aktulga, H. M.; Berger, R.; Bolintineanu, D. S.; Brown, W. M.; Crozier, P. S.; in 't Veld, P. J.; Kohlmeyer, A.; Moore, S. G.; Nguyen, T. D.; et al. LAMMPS - a flexible simulation tool for particle-based materials modeling at the atomic, meso, and continuum scales. *Comput. Phys. Commun.* **2022**, *271*, 108171.
(67) Maginn, E. J.; Messerly, R. A.; Carlson, D. J.; Roe, D. R.; Elliot, J. R. Best Practices for Computing Transport Properties 1. Self-Diffusivity and Viscosity from Equilibrium Molecular Dynamics [Article v1.0]. *Living Journal of Computational Molecular Science* **2018**, *1*, 6324.
(68) Yeh, I.-C.; Hummer, G. System-Size Dependence of Diffusion Coefficients and Viscosities from Molecular Dynamics Simulations with Periodic Boundary Conditions. *J. Phys. Chem. B* **2004**, *108*, 15873−15879.
(69) Gowers, R. J.; Linke, M.; Barnoud, J.; Reddy, T. J. E.; Melo, M. N.; Seyler, S. L.; Domanski, J.; Dotson, D. L.; Buchoux, S.; Kenney, I. M.; et al. MDAnalysis: A Python Package for the Rapid Analysis of Molecular Dynamics Simulations. *Proceedings of the 15th Python in Science Conference*; 2016; pp 98−105; DOI: 10.25080/Majora-629e541a-00e.
(70) Michaud-Agrawal, N.; Denning, E. J.; Woolf, T. B.; Beckstein, O. MDAnalysis: A toolkit for the analysis of molecular dynamics simulations. *J. Comput. Chem.* **2011**, *32*, 2319−2327.
(71) Gomer, R. Diffusion of adsorbates on metal surfaces. *Rep. Prog. Phys.* **1990**, *53*, 917.
(72) Kong, L. T.; Lewis, L. J. Transition state theory of the preexponential factors for self-diffusion on Cu, Ag, and Ni surfaces. *Phys. Rev. B* **2006**, *74*, 073412.
(73) Koettgen, J.; Zacherle, T.; Grieshammer, S.; Martin, M. Ab initio calculation of the attempt frequency of oxygen diffusion in pure and samarium doped ceria. *Phys. Chem. Chem. Phys.* **2017**, *19*, 9957−9973.

(74) Chen, B. W. J.; Kirvassilis, D.; Bai, Y.; Mavrikakis, M. Atomic and Molecular Adsorption on Ag(111). *J. Phys. Chem. C* **2019**, *123*, 7551−7566.
(75) Reiser, P.; Neubert, M.; Eberhard, A.; Torresi, L.; Zhou, C.; Shao, C.; Metni, H.; van Hoesel, C.; Schopmans, H.; Sommer, T.; Friederich, P.; et al. Graph neural networks for materials science and chemistry. *Communications Materials* **2022**, *3*, 93.
(76) Aljama, H.; Yoo, J. S.; Nørskov, J. K.; Abild-Pedersen, F.; Studt, F. Methanol Partial Oxidation on Ag(111) from First Principles. *ChemCatChem.* **2016**, *8*, 3621−3625.
(77) Nie, X.; Luo, W.; Janik, M. J.; Asthagiri, A. Reaction mechanisms of CO2 electrochemical reduction on Cu(111) determined with density functional theory. *J. Catal.* **2014**, *312*, 108−122.
(78) Kortlever, R.; Shen, J.; Schouten, K. J. P.; Calle-Vallejo, F.; Koper, M. T. M. Catalysts and Reaction Pathways for the Electrochemical Reduction of Carbon Dioxide. *J. Phys. Chem. Lett.* **2015**, *6*, 4073−4082.

https://doi.org/10.1021/acs.jpcc.4c02250
J. Phys. Chem. C 2024, 128, 13238−13248